nature structural & molecular biology

Brief Communication

https://doi.org/10.1038/s41594-023-01048-x

N⁶-adenosine methylation controls the translation of insulin mRNA

Received: 29 August 2022

Accepted: 26 June 2023

Published online: 24 July 2023

Check for updates

Daniel Wilinski 🗗 & Monica Dus 🗗 🖂

Control of insulin mRNA translation is crucial for energy homeostasis, but the mechanisms remain largely unknown. We discovered that insulin mRNAs across invertebrates, vertebrates and mammals feature the modified base N^6 -methyladenosine (m^6A). In flies, this RNA modification enhances insulin mRNA translation by promoting the association of the transcript with polysomes. Depleting m^6A in *Drosophila melanogaster insulin 2 mRNA* (dilp2) directly through specific 3' untranslated region (UTR) mutations, or indirectly by mutating the m^6A writer Mettl3, decreases dilp2 protein production, leading to aberrant energy homeostasis and diabetic-like phenotypes. Together, our findings reveal adenosine mRNA methylation as a key regulator of insulin protein synthesis with notable implications for energy balance and metabolic disease.

 m^6A is an abundant internal modification of eukaryotic mRNAs involved in regulating mRNA stability, turnover and translation 1,2 . Recent studies have implicated this pathway in the regulation of energy homeostasis and the pathogenesis of type 2 diabetes. Specifically, genetic depletion of m^6A levels in mammalian insulin β cells resulted in higher circulating glucose and diabetic phenotypes $^{3-5}$ and lower insulin-cell maturation in vitro 4 ; reduced m^6A levels were also observed in the pancreatic β cells of humans with type 2 diabetes 6,7 . Moreover, insulin biosynthesis is thought to be critically controlled at the translational level, but the mechanism remains uncharacterized 8,9 . Here, we took advantage of the ancestral conservation of the m^6A (ref. 10) and insulin systems in invertebrates 11 to identify the molecular mechanisms through which m^6A regulates glucose homeostasis and contributes to metabolic health.

In fruit flies (*Drosophila melanogaster*), 14 neuroendocrine cells in the pars intercerebralis (Fig. 1a) regulate hemolymph glycemia and energy homeostasis by producing three insulin-like hormones¹². Of these, the *Drosophila* insulin-like 2 peptide (dilp2), which has the highest homology to human insulin, is necessary and sufficient to regulate hemolymph glycemia and fat levels in adult flies^{11,13–15}. In line with this, mutations in the *dilp2* gene, or ablation of the insulin-producing cells, elevate hemolymph sugar and impair metabolic homeostasis, phenotypes rescued by injection of human insulin^{11–14}. The anatomical and genetic accessibility of the fly insulin cells makes this a uniquely suited system to investigate the in vivo function of the m⁶A pathway in energy homeostasis.

If the m⁶A pathway were important for energy balance in flies, we would expect that mutations in the conserved m⁶A methyltransferase writer *Mettl3*¹ would increase circulating glucose and fat-to-lean mass (Fig. 1a). Consistent with this, *Mettl3* homozygous loss-of-function mutants¹⁶ showed higher fasted circulating sugar levels (Fig. 1b) and triglycerides than control flies (Fig. 1c). These effects were rescued by expression of a wild-type *Mettl3* transgene only in the insulin-producing cells with *Dilp2-GAL4* and phenocopied by *Mettl3* knockdown exclusively in these cells (Fig. 1d–f and Extended Data Fig. 1a). Thus, *Mettl3* is specifically required in the fly insulin cells to regulate glucose and energy homeostasis. Importantly, these effects were not due to developmental alterations, as knocking down *Mettl3* only in posteclosion adult insulin cells (*dilp2>Mettl3*^{RNAi}; *tubulin-GAL80*^{ts}) resulted in the same phenotypes as *dilp2>Mettl3*^{RNAi} animals (Extended Data Fig. 1b).

The energy homeostasis phenotypes of *Mettl3*^{-/-} files are similar to those observed in *dilp2* mutants¹⁴; we thus examined the levels of *dilp2* mRNA and protein in *Mettl3*^{-/-} animals. We found no changes in the abundance of *dilp2* mRNA between homozygous *Mettl3*^{-/-} and control flies (Extended Data Fig. 2a), or in the mRNAs for *dilp3* and *dilp5*, the other insulin-like mRNAs produced in these cells (Extended Data Fig. 2b,c). However, there was a marked reduction in dilp2 protein in *Mettl3*^{-/-} mutant flies (Fig. 1g), without accompanying alterations in the number and morphology of the insulin cells or the amount of other dilp hormones (Extended Data Fig. 2d,e). m⁶A regulates RNA stability, turnover and translation in a context-dependent manner²; thus, lower dilp2 protein levels, in the absence of corresponding changes

Department of Molecular, Cellular, and Developmental Biology, The University of Michigan, Ann Arbor, MI, USA. 🖂 e-mail: mdus@umich.edu

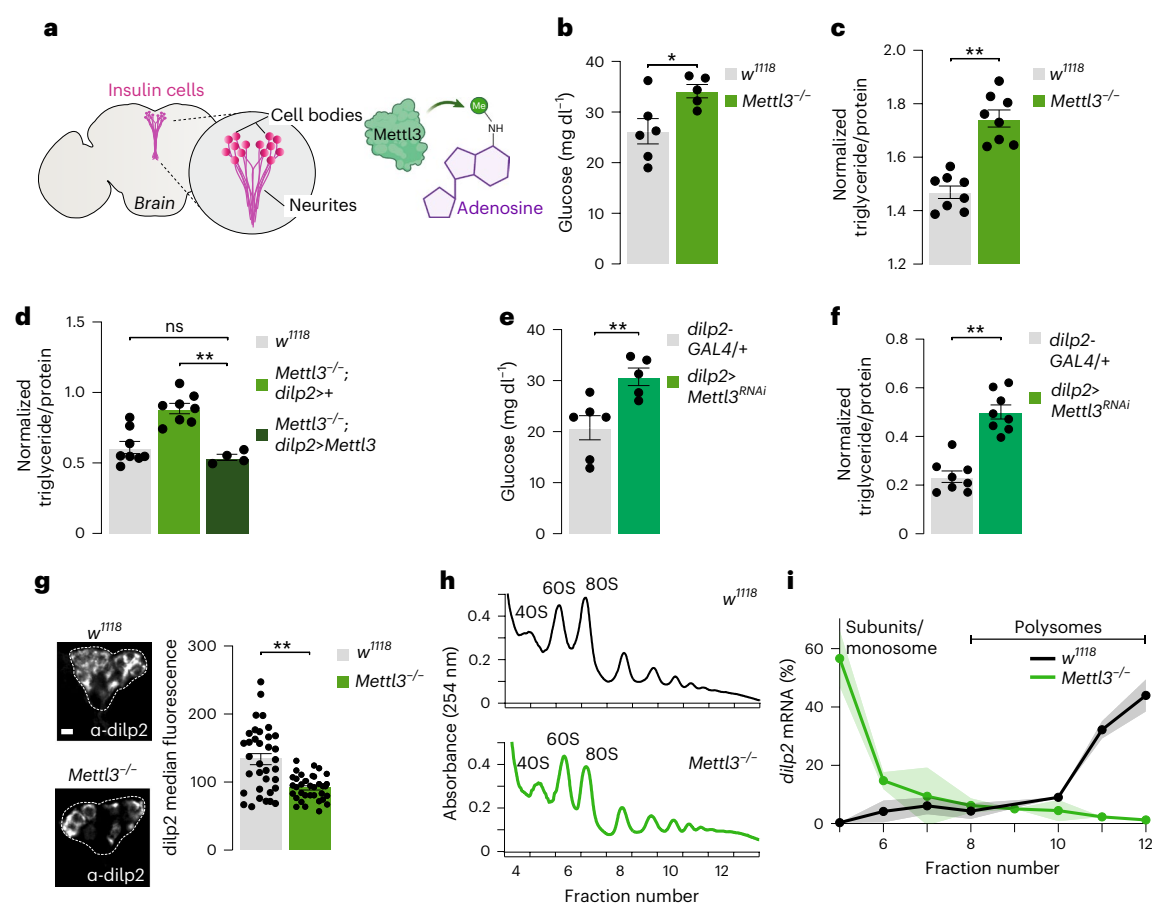


Fig. 1 | Mettl3 is required for glucose balance and energy homeostasis in the insulin-producing cells. a, Diagram showing the location and anatomy of insulin-producing cells in the fly brain and the methylation of adenosine by the Mettl3 protein. b, The circulating hemolymph glycemia (n = 6, 5) of fasted $Mettl3^{-/-}$ and $w^{IIIS}CS$ control flies. P = 0.027. c, Triglyceride levels normalized to protein in male $w^{IIIS}CS$ and mutant $Mettl3^{-/-}$ flies. n = 8; P < 0.0001. d, Triglyceride levels normalized to protein in male flies with cell-specific rescue of (dilp2>Mettl3) $Mettl3^{-/-}$ mutant flies. n = 8 pools of two flies; rescue flies n = 4. Two-way analysis of variance (ANOVA) with Tukey's multiple comparisons test. ns, not significant (0.387). Adjusted P = 0.0001. e, The hemolymph glycemia (n = 6) of starved $dilp2>Mettl3^{RNAi}$ and transgenic control flies. P = 0.009. f, Triglyceride levels normalized to protein in flies with cell-specific knockdown

of Mettl3 $(dilp2>Mettl3^{RNAi})$. n=8 pools of two flies; P<0.0001. **g**, Representative confocal images of immunofluorescence of dilp2 protein in control $(w^{IIIS}CS)$ and $Mettl3^{-/-}$ mutant flies. Scale bar, $20~\mu$ m. Quantification of median dilp2 fluorescence (arbitrary units) of individual insulin-producing cells from Mettl3 mutants and $w^{IIIS}CS$ control flies. n=15 brains. Male flies were starved for 16~h prior to dissection and collected in three independent sets. P<0.0001. **h**, Representative polysome profile from sucrose gradient of control $(w^{IIIS}CS)$ and $Mettl3^{-/-}$ mutant fly heads. **i**, The proportion of dilp2 mRNA in sucrose gradient fractions 5-12 normalized to spike-in RNA from control $(w^{IIIS}CS)$ and $Mettl3^{-/-}$ mutant flies. n=2, 400~heads per sample. Shading represents s.e.m. Unpaired two-tailed Student's t-test unless otherwise noted. *P<0.05; **P<0.005.

in mRNA abundance, could result from deficits in translation. To test this hypothesis, we fractionated polysomes from the heads of control and *Mettl3*^{-/-} mutants and measured the amount of *dilp2* transcript associated with each fraction (Fig. 1h,i). In control flies, 89% of the *dilp2* mRNAs cosedimented with polysome fractions, suggesting active and efficient translation (Fig. 1i, gray). Strikingly, this pattern was reversed in *Mettl3*^{-/-} flies, in which only 19% of *dilp2* mRNA was found in the heavier fractions; instead, 80% of this mRNA was associated with early fractions, representing individual ribosomal subunits and monosomes (Fig. 1i, green). Thus, m⁶A is required for the association of the *dilp2* mRNA with polysomes and the proper translation of the *dilp2* mRNA into protein. Of note, the 80S ribosome peak was lower in *Mettl3*^{-/-} flies, which could result in lower translation, as suggested by ref. 17 (Fig. 1h).

To understand how *Mettl3* mutations decrease *dilp2* translation, we used m⁶A ultraviolet light-induced crosslinking and immuno-precipitation (miCLIP) to uncover transcripts marked by m⁶A in fly heads¹⁸. The three miCLIP biological replicates demonstrated robust reproducibility with a mean correlation of 0.95 (Extended Data Fig. 3a) and revealed 4,506 m⁶A peaks corresponding to 1,828 genes involved

in brain processes such as development and plasticity (Extended Data Fig. 3b and Supplementary Data 1). Of these, 58% of transcripts coincided with those previously detected by m⁶A-CLIP and m⁶A RNA immunoprecipitation (m⁶A-RIP) in fly heads¹⁹, including the *Syntaxin 1A*, aaquetzalli, female lethal d, and pumilio genes (Supplementary Data 1). The majority of m⁶A peaks were located in the 5′ UTR of transcripts, whereas a substantial smaller fraction appeared in the 3′ UTR, particularly in close proximity to the stop codon (Extended Data Fig. 3c). These peaks were enriched in an RRAC (R, purine) sequence motif at C-to-T crosslinking-induced mutation sites (CIMS), which represent m⁶A sites from CLIP/RIP data¹⁶⁻¹⁹ (Extended Data Fig. 3d and Supplementary Data 1). In contrast to mammals^{20,21}, the location of m⁶As along the transcript and the modest sequence enrichment are consistent with previous reports in flies^{17,19}.

Among the regions methylated in vivo, we uncovered an m⁶A peak in the 3′ UTR of *dilp2* shortly after the stop codon (Fig. 2a); mRNAs for other insulin-like peptides *dilp3* and *dilp5* showed no methylation (Extended Data Fig. 3e,f). To better characterize the location of the modified adenosines in the *dilp2* mRNA, we turned to direct RNA

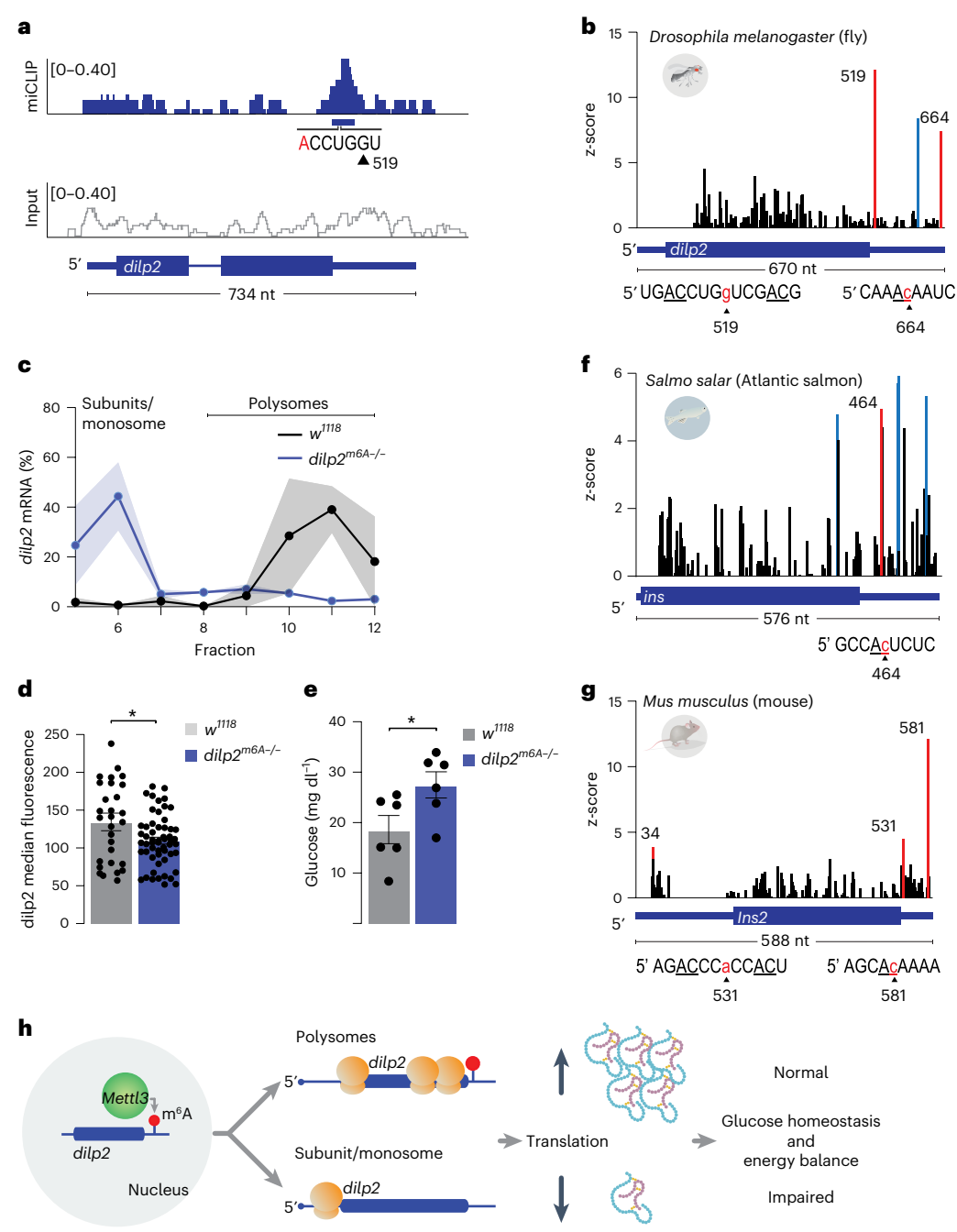


Fig. 2 | *Mettl3* is required for the translation of *dilp2* mRNA. a, miCLIP (top, blue) and the no immunoprecipitation input control (bottom, gray) traces mapped to the *dilp2* locus. The blue horizontal bar indicates the CLIP peak (false discovery rate (FDR) < 0.05) and the base composition flanking a putative m⁶A site near position 519. b, EpiNano significance trace showing the nucleotide positions that are significantly different (red or blue bars, z-score > 6) between native and in vitro transcribed *dilp2* RNAs. Red bars represent significantly different nucleotides near AC dinucleotides, and blue bars represent significant scores at nucleotides that do not contact ACs. Sequence context for positions 519 and 664 of *dilp2* are shown under the gene model. The sequence context for position 614 is in Supplementary Table 2. c, The proportion of *dilp2* mRNA in sucrose gradient fractions 5–12 normalized to spike-in RNA from control (*w*^{IIIB}CS) and *dilp2*^{m6A-/-} files. *n* = 2, 3 samples of 400 heads each. Shading represents s.e.m. d, Quantification of median dilp2 fluorescence of individual insulin-producing

cells from n=6 brains from control (w^{IJIS}) and $dilp2^{m6A-/-}$ mutant fly heads. Error bars represent s.e.m. Unpaired two-tailed Student's t-test, P=0.021. **e**, The circulating hemolymph glycemia (n=6) of fasted $dilp2^{m6A-/-}$ and w^{IJIS} control flies. Error bars represent s.e.m. Unpaired two-tailed Student's t-test, P=0.042. **f**, **g**, Direct RNA sequencing significance trace comparing in vitro transcribed salmon ins (**f**) or mouse Ins2 (**g**) RNA to native mRNA isolated from salmon pancreatic tissue (**f**) or mouse pancreatic islets (**g**). Red or blue bars represent the significantly different nucleotides near AC dinucleotides (red) or not at AC nucleotides (blue) (z-scores > 4 or >5) between native and in vitro transcribed RNAs. Sequence context for positions ins 464 and Ins2 531 and 581 are shown under the gene model. Sequence context for the remaining positions is in Supplementary Table 2. **h**, Model of translational control of dilp2 mRNA by m⁶A. *P<0.005; **P<0.005.

sequencing (Oxford Nanopore), in which different bases are identified by changes in current flow through nanopores^{22–24}. To first ensure that we could faithfully detect the presence of methylated A, we sequenced

in vitro transcribed RNAs with only one methylated or unmethylated A (position 239) and used EpiNano to detect the modified A (Extended Data Fig. 4a); this algorithm identifies m⁶As by detecting deviations

in base calls caused by current intensity changes between modified and unmodified nucleotides²³. Indeed, EpiNano flagged the current shift near A239 (Extended Data Fig. 4b) as a base-calling deviation (Extended Data Fig. 4c), showing that it can reliably detect methylated A. To identify m⁶As in the native dilp2 mRNA from fly heads, we first enriched for transcripts specifically expressed in the insulin-producing cells by translating ribosome affinity purification (TRAP) (Dilp2-GAL4 >RPL3::FLAG²⁵). We then direct RNA sequenced the immunoprecipitated poly(A) + RNA and used EpiNano to detect deviations between base calls of in vitro transcribed and native *dilp2* RNA²³. This analysis uncovered a significant difference in the 3' UTR between the in vitro transcribed and native dilp2 mRNAs (Fig. 2b and Extended Data Fig. 4d), with three bases in the 3' UTR (positions G519, C614 and C664) showing significantly higher base-call deviations. Position G519 is near a putative methylated AC contained within the CLIP peak, and position C664 is part of AC dinucleotides (Fig. 2b and Supplementary Table 2). The remaining peak did not include an AC and is therefore unlikely to be methylated (Supplementary Table 2). Together with the results from miCLIP, the direct RNA sequencing results show that at least two specific ACs in the 3' UTR of the dilp2 mRNA are methylated in vivo in D. melanogaster.

To investigate whether m⁶A of the dilp2 3' UTR directly affected its translation, we generated transgenic flies that lacked 'methylatable' adenosines in the 3' UTR ($dilp2^{m6A-/-}$). Guided by the miCLIP and direct RNA sequencing analyses, we selected 11 AC nucleotides to mutate into UC (Extended Data Fig. 5a), including the ACs near G519 with the strongest methylation signal (Fig. 2a,b); A663 could not be removed for technical reasons. Transgenic fly line 236-4 was selected for further study after confirming all A>U mutations by Sanger sequencing (Extended Data Fig. 5b). In control flies matched to the genetic background of the dilp2^{m6A-/-} mutants, 90% of the dilp2 mRNAs were in the heavier polysome fractions; however, in *dilp2*^{m6A-/-} flies, 74% of *dilp2* mRNAs were associated with early fractions (Fig. 2c and Extended Data Fig. 6a,b). Importantly, the ratios of 60S and 80S ribosomes were similar between control and mutant files, showing that the effect on dilp2 translation is direct and not due to overall changes in translation (Extended Data Fig. 6a,b). Consistent with this, quantification of the total levels of dilp2 protein with anti-dilp2 antibodies in the insulin cells of fasted flies revealed a ~20% decrease in *dilp2*^{m6A-/-} mutants compared with genetic background controls (Fig. 2d and Extended Data Fig. 6c). Strikingly, dilp2^{m6A-/-} mutants recapitulated the deficits in glucose and energy homeostasis observed in Mettl3 mutant flies, with an increase in fasting glucose levels and triglycerides (Fig. 2e and Extended Data Fig. 6d). Thus, m⁶A modification of the dilp2 mRNA directly controls the effective translation, and thus synthesis, of the insulin hormone in flies.

Elements in the 3' UTR of mammalian insulin are thought to play an important role in its translation^{8,9}. Given the conservation of the insulin and m⁶A pathways in metazoa, we asked if signatures of m⁶A were also present in vertebrate insulin mRNAs. We obtained poly(A)-selected mRNAs from Atlantic salmon (Salmo salar) pancreatic tissue and mouse (Mus musculus) pancreatic islet cells and examined them by direct RNA sequencing. EpiNano analysis of 5,000 and 10,000 reads mapped to the ins (salmon) and Ins2 (mouse) insulingenes identified three sites with base-call deviations within three bases from AC dinucleotides in the 3' UTR of both genes: C464 for salmon ins (5' GCCAc464UCUC) (Fig. 2f and Supplementary Table 2) and A531 (5' AGACCCa531CCACU) and C581 (5' AGCAc581AAAA) for mouse Ins2 (Fig. 2g and Supplementary Table 2); base-call deviations not near AC dinucleotides are listed in Supplementary Table 2. To corroborate the direct RNA sequencing data, we enriched for m⁶A methylated mRNAs from these tissues and assayed for insulin mRNAs by quantitative PCR (m⁶A-RIP-qPCR). This resulted in a robust enrichment of insulin mRNAs compared with no-antibody controls for salmon ins and mouse Ins2 pancreatic mRNA (Extended Data Fig. 7a,b). Thus, like the fly dilp2, vertebrate insulin mRNAs are marked by m⁶A sites in the 3' UTR. Finally, to examine if human insulin (INS) mRNA was also methylated, we analyzed recently published RIP sequencing data from pancreatic islets⁶. Consistent with our vertebrate data, we observed an enrichment in INS mRNA reads in the m⁶A-RIP compared with input (Extended Data Fig. 7c).

Taken together, our data and analyses indicate that N^6 -adenosine methylation of insulin mRNAs is conserved from flies to humans. We propose that this RNA modification controls the synthesis of the insulin protein (Fig. 2h). This idea is directly supported by experiments in flies, in which methylation of specific adenosines near the stop codon enhanced translation by promoting the association of the transcript with polysomes. To this end, previous studies have shown that enhanced physiological translation of the mammalian insulin transcript depends on regulatory elements in the 3'UTR, but the mechanisms are not understood^{8,9}. In our experiments, dilp2 mRNAs without m⁶A marks in their 3' UTR remained associated with the 40S ribosome fractions, suggesting that this modification is important for translational initiation. As m⁶A levels have been linked to cellular $metabolism \, and \, signaling^{2,26}, this \, epitranscriptomic \, mark \, in \, the \, insulin$ 3' UTR could tie translation with specific physiological signals, such as glucose influx or depolarization.

Beyond discovering a new mechanism that controls insulin translation, our work also uncovers a specific cause for the alterations in glucose homeostasis observed in mammals with mutations in the m⁶A complex^{4-6,27}. As with mice, flies with loss-of-function mutations in *Mettl3* or with knockdown of this enzyme in the insulin cells had marked deficits in energy homeostasis, including high glycemia. These phenotypes were recapitulated in flies with 'unmethylatable' *dilp2* mRNA, showing that these alterations in energy balance directly arise from impaired insulin translation. However, we do not exclude that additional mRNA targets may be involved. For example, we found m⁶A signatures in mRNAs that are also methylated in human islet cells and/or murine tissues and could play a role in energy homeostasis^{6,28}, such as *Hexokinase A* (*Hex-A*), *Phosphatase and tensin homolog* (*Pten*), and *forkhead box*, *sub-group O* (*Foxo*).

In conclusion, our work unveils a fundamental role for RNA methylation in the synthesis of insulin and the control of energy homeostasis. Future studies combining the unique advantages of invertebrate and vertebrate models will advance our understanding of the role of epitranscriptomics and translation control in metabolism, with critical implications for the prevention and treatment of chronic diseases.

Online content

Any methods, additional references, Nature Portfolio reporting summaries, source data, extended data, supplementary information, acknowledgements, peer review information; details of author contributions and competing interests; and statements of data and code availability are available at https://doi.org/10.1038/s41594-023-01048-x.

References

- Zaccara, S., Ries, R. J. & Jaffrey, S. R. Reading, writing and erasing mRNA methylation. Nat. Rev. Mol. Cell Biol. 20, 608–624 (2019).
- He, P. C. & He, C. m⁶A RNA methylation: from mechanisms to therapeutic potential. *EMBO J.* 40, e105977 (2021).
- Men, L., Sun, J., Luo, G. & Ren, D. Acute deletion of METTL14 in β-cells of adult mice results in glucose intolerance. *Endocrinology* 160, 2388–2394 (2019).
- Liu, J. et al. METTL14 is essential for β-cell survival and insulin secretion. Biochim. Biophys. Acta Mol. Basis Dis. 1865, 2138–2148 (2019).
- Li, X., Yang, Y. & Chen, Z. Downregulation of the m⁶A reader protein YTHDC1 leads to islet β-cell failure and diabetes. Metabolism 138, 155339 (2023).
- De Jesus, D. F. et al. m⁶A mRNA methylation regulates human β-cell biology in physiological states and in type 2 diabetes. *Nat. Metab.* 1, 765–774 (2019).

- Yang, Y. et al. Glucose is involved in the dynamic regulation of m⁶A in patients with type 2 diabetes. J. Clin. Endocrinol. Metab. 104, 665–673 (2019).
- 8. Jahr, H., Schröder, D., Ziegler, B., Ziegler, M. & Zühlke, H. Transcriptional and translational control of glucose-stimulated (pro)insulin biosynthesis. *Eur. J. Biochem.* **110**, 499–505 (1980).
- Magro, M. G. & Solimena, M. Regulation of β-cell function by RNA-binding proteins. *Mol. Metab.* 2, 348–355 (2013).
- Lence, T., Soller, M. & Roignant, J.-Y. A fly view on the roles and mechanisms of the m⁶A mRNA modification and its players. RNA Biol. 14, 1232–1240 (2017).
- Das, R. & Dobens, L. L. Conservation of gene and tissue networks regulating insulin signalling in flies and vertebrates. *Biochem.* Soc. Trans. 43, 1057–1062 (2015).
- Rulifson, E. J., Kim, S. K. & Nusse, R. Ablation of insulin-producing neurons in flies: growth and diabetic phenotypes. Science 296, 1118–1120 (2002).
- 13. Kannan, K. & Fridell, Y.-W. C. Functional implications of *Drosophila* insulin-like peptides in metabolism, aging, and dietary restriction. *Front. Physiol.* **4**, 288 (2013).
- Semaniuk, U. V. et al. Insulin-like peptides regulate feeding preference and metabolism in *Drosophila*. Front. Physiol. 9, 1083 (2018).
- Brogiolo, W. et al. An evolutionarily conserved function of the Drosophila insulin receptor and insulin-like peptides in growth control. Curr. Biol. 11, 213–221 (2001).
- Lence, T. et al. m⁶ A modulates neuronal functions and sex determination in *Drosophila*. *Nature* 540, 242–247 (2016).
- Kan, L. et al. The m⁶A pathway facilitates sex determination in Drosophila. Nat. Commun. 8, 15737 (2017).
- Grozhik, A. V., Linder, B., Olarerin-George, A. O. & Jaffrey, S. R. Mapping m⁶ A at individual-nucleotide resolution using crosslinking and immunoprecipitation (miCLIP). *Methods Mol. Biol.* 1562, 55–78 (2017).
- Kan, L. et al. A neural m⁶A/Ythdf pathway is required for learning and memory in *Drosophila*. Nat. Commun. 12, 1458 (2021).

- Dominissini, D. et al. Topology of the human and mouse m⁶A RNA methylomes revealed by m⁶A-seq. *Nature* 485, 201–206 (2012).
- Meyer, K. D. et al. Comprehensive analysis of mRNA methylation reveals enrichment in 3' UTRs and near stop codons. Cell 149, 1635–1646 (2012).
- 22. Garalde, D. R. et al. Highly parallel direct RNA sequencing on an array of nanopores. *Nat. Methods* **15**, 201–206 (2018).
- 23. Liu, H. et al. Accurate detection of m⁶A RNA modifications in native RNA sequences. *Nat. Commun.* **10**, 4079 (2019).
- Parker, M. T. et al. Nanopore direct RNA sequencing maps the complexity of Arabidopsis mRNA processing and m⁶A modification. eLife 9, e49658 (2020).
- Chen, X. & Dickman, D. Development of a tissue-specific ribosome profiling approach in *Drosophila* enables genomewide evaluation of translational adaptations. *PLoS Genet.* 13, e1007117 (2017).
- Kim, J. & Lee, G. Metabolic control of m⁶A RNA modification. Metabolites 11, 80 (2021).
- Li, X., Jiang, Y., Sun, X., Wu, Y. & Chen, Z. METTL3 is required for maintaining β-cell function. Metabolism 116, 154702 (2021).
- Zhong, H., Tang, H.-F. & Kai, Y. N6-methyladenine RNA modification (m⁶A): an emerging regulator of metabolic diseases. *Curr. Drug Targets* 21, 1056–1067 (2020).

Publisher's note Springer Nature remains neutral with regard to jurisdictional claims in published maps and institutional affiliations.

Springer Nature or its licensor (e.g. a society or other partner) holds exclusive rights to this article under a publishing agreement with the author(s) or other rightsholder(s); author self-archiving of the accepted manuscript version of this article is solely governed by the terms of such publishing agreement and applicable law.

© The Author(s), under exclusive licence to Springer Nature America, Inc. 2023

Methods

Fly lines and husbandry

All flies were maintained at 25 °C in a humidity-controlled incubator with a 12 h/12 h light/dark cycle. Animals were fed Bloomington Food B (cornmeal-glucose) ad libitum and provided fresh food every other day. For all experiments, flies were collected under $\rm CO_2$ anesthesia 2–4 days following eclosion, and housed in groups of 20–30 to age until testing (6–10 days old). The stocks used are listed in Supplementary Table 3. The *Mettl3* null mutants were backcrossed six times to w^{III8} *Canton-S* (w^{III8} CS) flies (Benzer Laboratory, California Institute of Technology) and compared with this genetic control, whereas $Dilp2^{m6A}$ mutants were generated in the w^{III8} background and compared with it (Rainbow Transgenic Flies).

RNA extraction

Standard methods to isolate total RNA were used for qPCR, CLIP and direct RNA sequencing. In brief, heads from 10–20 flies were dissected and immediately frozen on dry ice for qPCR. Eight hundred fly heads were isolated from bodies by sieving for CLIP and direct RNA sequencing. All samples were stored at $-80\,^{\circ}$ C until extraction. Phenol–chloroform (Invitrogen, 15596018) and RIPA buffer (150 mm NaCl, 1% Nonidet P-40 (NP-40), 0.5% sodium deoxycholate, 0.1% SDS, 50 mM Tris pH 7.5) were added to frozen samples and homogenized by bead bashing (Bead Ruptor, Omni, 19-040E). RNA extracted by phenol–chloroform was precipitated by isopropanol with GlycoBlue coprecipitant (Invitrogen, AM9515). RNA was stored at $-80\,^{\circ}$ C until further processing.

Crosslinking immunoprecipitation (CLIP)

Library preparation. We adapted miCLIP¹⁸ to use infrared-dyeconjugated irCLIP adaptors²⁹. In brief, 20 µg of poly(A)-selected (Invitrogen, 61012) RNA for each biological replicate from 800 heads of $w^{1118}CS$ flies was used as input to the CLIP, no-antibody control, and input-only (no-CLIP) reactions. Fragmented RNA (Ambion, E6150S) was incubated for 2 h at 4 °C with 10 μl of antibody against m⁶A (Abcam, ab151230), UV-crosslinked, then immunoprecipitated with magnetic beads (Invitrogen, 10004D) as in ref. 18. Pre-adenylated dye-conjugated linkers were ligated (New England Biolabs, M0351S) to dephosphorylated 3' ends of RNA fragments overnight at 16 °C (Supplementary Table 1). RNA was extracted with NuPAGE SDS buffer and separated by NuPAGE gel (Invitrogen, NP0321), transferred to nitrocellulose membrane and visualized for excision at 800 nm. RNA-antibody complexes were released from the membrane by proteinase K digestion, and RNA was purified with phenol-chloroform extraction. RNA was reverse transcribed (Invitrogen, 18080085), circularized (Lucigen, CL4111K) and PCR-amplified (Thermo Scientific, F530S) following the published protocol¹⁸. Libraries were subjected to 151 bp paired-end sequencing according to the manufacturer's protocol on an Illumina NovaSeq 6000 at the University of Michigan Genomics Core.

Bioinformatics. Sequencing reads were demultiplexed using bcl2fastq2 Conversion Software (Illumina). 5'-end unique molecular identifiers (UMIs; 9 nucleotide (nt) random sequence) were used to remove PCR duplicates with a custom script. Then, UMIs, sequences and sequencing adapters were removed (fastx_clipper v0.0.14). Reads were mapped to the Ensembl D. melanogaster genome (BDGP6) using STAR (v2.7.5a)³⁰ with default settings (Supplementary Table 4). Aligned reads were peak-called using Piranha (v1.2.1)³¹ (Supplementary Data 1). Metagene analysis was performed using MetaPlotR³². Pearson's correlation coefficient (r) was calculated using R. CIMS analysis was performed as in ref. 18. The sequence logo was generated using WebLogo (v2.8.2)³³. Gene ontology (GO) analysis was performed using gene set enrichment analysis (GSEA) implemented in the cluster Profiler R package v4.2.2³⁴. We used the Benjamini-Hochberg method to correct for multiple hypothesis testing, and 'biological process' from the org.Dm.eg.db Bioconductor package v3.8.2 for GSEA³⁵.

Polysome fractionation

Polysome profiles were performed as previously described³⁶. In brief. 300 fly heads were homogenized using a bead beater (Omni, 19-040E) in 800 µl of polysome extraction buffer (300 mM NaCl, 50 mM Tris-HCl pH7.5, 10 mM MgCl₂, 200 mg ml⁻¹heparin, 400 U ml⁻¹RNasin, 1.0 mM phenylmethylsulfonyl fluoride, 0.2 mg ml⁻¹ cycloheximide, 1% Triton X-100, 0.1% sodium deoxycholate), then incubated for 10 min on ice. Lysate was cleared by centrifugation at $10,000 \times g$ for 10 min at 4 °C. Equal A260 units were layered onto a 10-50% sucrose gradient in resolving buffer (20 mM Tris-HCl pH 7.5, 150 mM NaCl, 15 mM MgCl₂, 1 mM DTT, 100 µg ml⁻¹ cycloheximide) and separated using a Beckman SW 41 Ti rotor (30,000 r.p.m. for 3 h at 4 °C). The absorbance (254 nm) was monitored, and 750 µl fractions were collected using a Brandel pump set to a flow rate of 1.5 ml min⁻¹. Equal molar concentrations of Saccharomyces cerevisiae enolase-2 (Eno2) transcript were added to all fractions before RNA isolation. Nucleic acid was precipitated from each fraction, and pellets were then resuspended in water and extracted using phenol-chloroform, following the manufacturer's protocol (Invitrogen, 15596026). The RNA was precipitated with isopropanol and GlycoBlue. RNA was resuspended in 10 µl of water, and equal volumes from each fraction were reverse transcribed following the manufacturer's recommendations (Invitrogen, 18080085). Fractions 5-12 were probed for dilp2 and Eno2 RNA by qPCR (Supplementary Table 1).

qPCR

Reverse transcription was performed using SuperScript III (Invitrogen, 18080085) with 1 μ g of total RNA as input and primed with oligo(dT) (Invitrogen, 18418012) according to the manufacturer's protocol for transcript abundance analysis. qPCR was performed following the manufacturer's directions (Applied Biosystems, 4367659) for all experiments. Primers were added at a concentration of 2.5 μ M in 20 μ I reactions. Reactions were run on the StepOnePlus Real-Time PCR System (Applied Biosystems), and quantifications were normalized relative to the reference gene ribosomal protein 49 (*Rp49*) for transcript abundance or spike-in, *Eno2*, for polysome fractionation (delta Ct method).

Fat and lean mass analysis

Colorimetric measurements of triglycerides (Stanbio, SB-2100-430) and protein (Pierce, PI23225) were done as previously described 37 , where one biological replicate n=2 male flies. Flies were collected 3–5 days after eclosion and homogenized with a Bead Ruptor. Standard curves were generated for each to normalize the concentration of the samples. Samples were quantified using a Tecan Spark plate reader at 562 nm for protein or 500 nm for triglycerides.

Immunofluorescence

Immunofluorescence was done essentially as in ref. 38. Male flies 3–5 days after eclosion were sorted, then aged for 2–5 days on standard food. Flies were then fasted in vials with a wetted Kimwipe for 16–18 h before dissection. Brains were dissected in PBS, fixed (4% paraformal-dehyde aqueous solution in 1x PBS), blocked (10% normal goat serum, 2% Triton X-100, 1x PBS), and then incubated overnight in primary anti-body (rat anti-dilp2 (1:500)³⁹, rabbit anti-dilp3 (1:500)⁴⁰). After washing (3% NaCl, 1% Triton X-100, 1x PBS), brains were incubated overnight at 25 °C in secondary antibody: either goat anti-rat Alexa Fluor 647 (Invitrogen, A-21247) or goat anti-rabbit Alexa Fluor 488 (Invitrogen, A-11008). Brains were mounted in Focus Clear (CelExplorer, FC-101) on coverslips, and the cell bodies were imaged using an Olympus FV1200 confocal microscope with a ×20 objective. The median intensity of individual insulin-producing cells was quantified using Fiji⁴¹.

In vitro transcription for direct RNA sequencing

DNA insulin templates were synthesized by Integrated DNA Technologies based on transcripts FBtr0076329 (fly *Dilp2*) and NM_001185083.2 (mouse *Ins2*), as well as two randomized sequences containing only one

adenine (Supplementary Table 2). To generate the salmon *ins* template, we PCR-amplified (Thermo Scientific, F530S) from complementary DNA and Sanger sequence-verified the product ($XM_014198195.2$). Each template DNA sequence was used for in vitro transcription (Invitrogen, AM1334). To generate the randomized DNA template 'rand-A', the reaction mixture contained bases adenosine, uracil, cytosine and guanosine, whereas the randomized DNA template 'rand-m⁶A' used N^6 -methyladenosine in the place of adenosine. All other in vitro transcription reactions used only the standard bases. The reactions were performed overnight following the manufacturer's protocol.

Direct RNA sequencing

RNA was immunoprecipitated from the heads of flies expressing Dilp2-GAL4 UAS-RpL3::FLAG transgene (TRAP) as previously reported 42 with anti-Flag antibody (Sigma, F1804) (3 µg). RNA was extracted using phenol-chloroform (TRIzol), then poly(A)-selected (Invitrogen, 61011). RNA from Atlantic salmon pancreatic tissue and mouse islet cells were poly(A)-selected. Poly(A)-selected RNA or a total of 500 ng of pooled in vitro transcribed RNA was used for library preparation following the manufacturer's protocol (Oxford Nanopore, SQK-RNA002, vDRS_9080_v2_revB_22Nov2018). In brief, the reverse transcriptase adapter was ligated to the RNA, reverse transcription was performed, and the RNA-cDNA hybrids were purified. Next, the second adapter was ligated to the RNA, and the hybrids were again purified. The libraries were loaded onto the MinION flow cell (R9.4.1). The Oxford Nanopore sequencer was run for 24-36 h. Data were base-called using Oxford Nanopore's Guppy (v3.1.5) and aligned to the reference sequences using Minimap2 -ax splice -uf -k14 (v2.17)43. Only reads that passed filtering and that mapped to the reference were considered for further analysis. Next, aligned reads from biological samples (modified) and matched in vitro transcribed RNAs (unmodified) were used as input to EpiNano (EpiNano-Error, v1.2) to determine the positions of modifications²³. We plotted the data from the longest transcript (NM_001185083.2) for EpiNano mouse data. The Tombo suite of tools was used to visualize reads44.

Circulating glucose assay

Hemolymph was collected by centrifugation from 40–50 starved (12–16 h) male flies per replicate. Circulating glucose levels were measured as previously described ⁴⁵. In brief, 0.5 μ l of hemolymph was added to 100 μ l of HexoKinase (HK) reagent (Sigma, GAHK20) and incubated for 15 min at room temperature. Then, absorbance at 340 nm was measured on a Tecan Spark plate reader.

Generation of dilp2 m⁶A mutant flies

CRISPR constructs were synthesized and micro-injected into $w^{\rm III8}$ flies by Rainbow Transgenic Flies. The pScarless donor vector (dsRed marker) was introduced to remove the endogenous $dilp2\,3'$ UTR and replace it with a mutant $dilp2\,3'$ UTR that replaced 11 AC dinucleotides to TC (Extended Data Fig. 4a). F_1 progeny were screened for transformation with dsRed fluorescence. Positive transformants were Sanger sequenced (see Sanger sequencing) to verify the correct insertion.

Sanger sequencing

Genomic DNA was extracted by silica column purification (Invitrogen, K182002) from two male flies from each fly line with positive dsRed expression. The dilp2 locus was PCR-amplified (Thermo Scientific, F-530XL), and PCR products were purified and normalized to 5 ng μl^{-1} with 10 pmol μl^{-1} of the appropriate primer added. Samples were submitted to Eurofins Genomics for sequencing, and traces were analyzed with Benchling software.

Mouse islet isolation

Islet cells were collected from two to four fasted male mice from Vil-Cre backcrossed nine times to C57 by the University of Michigan

Islet Isolation Core. The pooled tissue was added directly to TRIzol (Invitrogen, 15596018) and stored at $-80\,^{\circ}$ C.

Salmon pancreatic tissue isolation

The Atlantic salmon used was approximately 2 years old and postsmolt. The pancreatic tissue from one individual was isolated from the surrounding pyloric caeca. Upon removal, the tissue was immediately added to TRIzol and stored at -80 °C.

m^6A methylated RNA immunoprecipitation qPCR (m^6A -RIP-qPCR)

Poly(A)-selected (Invitrogen, 61011) RNA was incubated with IgG Dynabeads (Invitrogen) (mock) or beads pre-incubated with antibody against m 6 A (Abcam, ab151230) for 2 h at 4 °C, then washed with binding buffer (150 mM NaCl, 10 mM Tris-HCl pH 7.5, 0.1% NP-40). RNA was eluted with 100 µl of 20 mM m 6 A (Sigma, M2780) for 2 h at 4 °C and then purified following the manufacturer's protocol (TRIzol, Invitrogen). qPCR was performed as above with 10% of the starting material as input. The normalized Ct values were calculated as follows: Ct of mock RIP or RIP – adjusted Ct of input. All primers are listed in Supplementary Table 1. Previously published data from human m 6 A RIP sequencing were obtained from the Gene Expression Omnibus (GEO; accession number GSE120024) 6 . Normalized counts of transcripts per kilobase million (TPM) for INS were precomputed by GEO2R, and two-way paired t-test was performed in GraphPad Prism.

Statistics and reproducibility

No statistical method was used to predetermine sample size. No data were excluded from the analyses. The experimental groups were randomized, and the investigators were blinded when determining regions of interest for fluorescence measurements, but not during experiments and outcome assessment.

Reporting summary

Further information on research design is available in the Nature Portfolio Reporting Summary linked to this article.

Data availability

All data are available in the main text or supplementary materials. RNA sequencing reads were deposited in GEO under accession number GSE207547. *dilp23′* UTR mutants are available upon request. The *D. melanogaster* genome sequence is available in Ensembl under BDGP6.32, *Mus musculus Ins2* is available in GenBank under NM_001185083.2, and *Salmo salar ins* is available in GenBank under XM_014198195.2. Source data are provided with this paper.

Code availability

All custom scripts for data analysis can be found at https://github.com/dwilinski/m6A-fly-insulin.git.

References

- Zarnegar, B. J. et al. irCLIP platform for efficient characterization of protein–RNA interactions. *Nat. Methods* 13, 489–492 (2016).
- 30. Dobin, A. et al. STAR: ultrafast universal RNA-seq aligner. *Bioinformatics* **29**, 15–21 (2013).
- 31. Uren, P. J. et al. Site identification in high-throughput RNA-protein interaction data. *Bioinformatics* **28**, 3013–3020 (2012).
- 32. Olarerin-George, A. O. & Jaffrey, S. R. MetaPlotR: a Perl/R pipeline for plotting metagenes of nucleotide modifications and other transcriptomic sites. *Bioinformatics* **33**, 1563–1564 (2017).
- 33. Crooks, G. E., Hon, G., Chandonia, J.-M. & Brenner, S. E. WebLogo: a sequence logo generator. *Genome Res.* **14**, 1188–1190 (2004).
- Yu, G., Wang, L.-G., Han, Y. & He, Q.-Y. clusterProfiler: an R package for comparing biological themes among gene clusters. OMICS 16, 284–287 (2012).

- Carlson, M. org.Dm.eg.db: genome wide annotation for Fly. Bioconductor https://doi.org/10.18129/B9.BIOC.ORG.DM.EG.DB (2017).
- Essers, P. et al. Reduced insulin/insulin-like growth factor signaling decreases translation in *Drosophila* and mice. *Sci. Rep.* 6, 30290 (2016).
- Wilinski, D. et al. Rapid metabolic shifts occur during the transition between hunger and satiety in *Drosophila melanogaster*. Nat. Commun. 10, 4052 (2019).
- May, C. E. et al. High dietary sugar reshapes sweet taste to promote feeding behavior in *Drosophila melanogaster*. *Cell Rep.* 27, 1675–1685.e7 (2019).
- 39. Géminard, C., Rulifson, E. J. & Léopold, P. Remote control of insulin secretion by fat cells in *Drosophila*. *Cell Metab*. **10**, 199–207 (2009).
- 40. Buhler, K. et al. Growth control through regulation of insulin signalling by nutrition-activated steroid hormone in *Drosophila*. *Development* **145**, dev165654 (2018).
- 41. Schindelin, J. et al. Fiji: an open-source platform for biological-image analysis. *Nat. Methods* **9**, 676–682 (2012).
- 42. Vaziri, A. et al. Persistent epigenetic reprogramming of sweet taste by diet. Sci. Adv. **6**, eabc8492 (2020).
- Li, H. Minimap2: pairwise alignment for nucleotide sequences. Bioinformatics 34, 3094–3100 (2018).
- 44. Stoiber, M. et al. De novo identification of DNA modifications enabled by genome-guided nanopore signal processing. Preprint at *bioRxiv* https://doi.org/10.1101/094672 (2017).
- 45. Tennessen, J. M., Barry, W. E., Cox, J. & Thummel, C. S. Methods for studying metabolism in *Drosophila*. *Methods* **68**, 105–115 (2014).

Acknowledgements

We thank P. Léopold (Institut Curie) for the kind gift of the dilp2 antibody, P. Callaerts (KU Leuven) for the gift of the dilp3 antibody, R. Seeley and C. Cras-Méneur for mouse islets (University of Michigan), B. Peterson (National Cold Water Marine Aquaculture Center) for salmon tissue, J.-Y. Roignant (University of Lausanne) for *Mettl3* mutant flies, and the Bloomington Drosophila Stock Center for other flies used in this study. We are grateful to P. Todd and S. Miller for training

and the use of their polysome fractionation equipment, C. Lapointe for thoughtful comments on the manuscript, and C. Duan for advice. We also thank J. Kuhl for designing some of the graphics in this manuscript. This work was supported by National Institutes of Health grants ROO DK-097141 (M.D.), 1DP2DK-113750 (M.D.), T32 DA007268 (D.W.), P30 DK089503 (M.D. and D.W.), and K99 DK128539 (D.W.); the Rita Allen Foundation (M.D.); and National Science Foundation CAREER 1941822 (M.D.).

Author contributions

Conceptualization: D.W. and M.D. Methodology: D.W. Investigation: D.W. and M.D. Visualization: D.W. and M.D. Funding acquisition: M.D. and D.W. Project administration: M.D. Supervision: M.D. Writing – original draft: D.W. and M.D. Writing – review & editing: D.W. and M.D.

Competing interests

The authors declare no competing interests.

Additional information

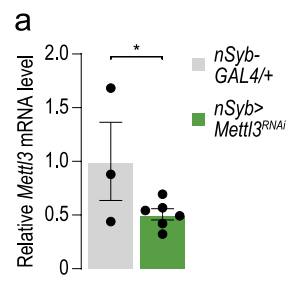
Extended data is available for this paper at https://doi.org/10.1038/s41594-023-01048-x.

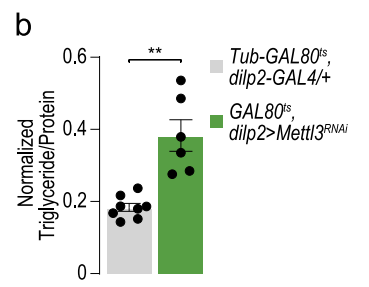
Supplementary information The online version contains supplementary material available at https://doi.org/10.1038/s41594-023-01048-x.

Correspondence and requests for materials should be addressed to Monica Dus.

Peer review information *Nature Structural & Molecular Biology* thanks the anonymous reviewers for their contribution to the peer review of this work. Carolina Perdigoto and Dimitris Typas were the primary editors on this article and managed its editorial process and peer review in collaboration with the rest of the editorial team. Peer reviewer reports are available.

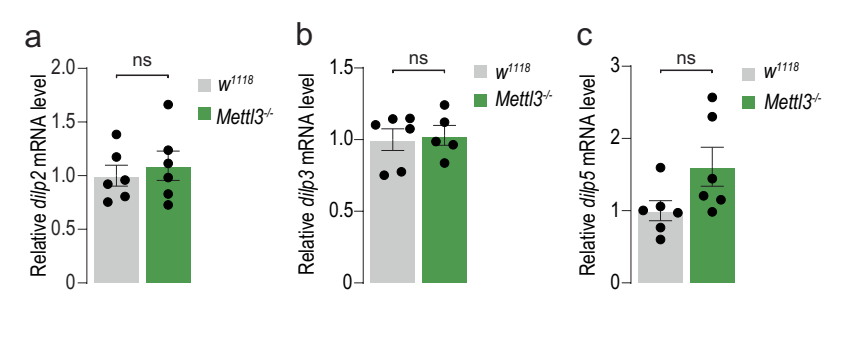
Reprints and permissions information is available at www.nature.com/reprints.

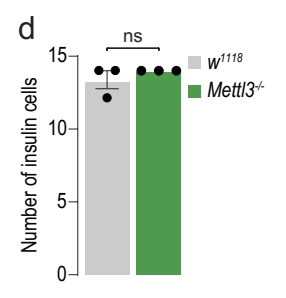


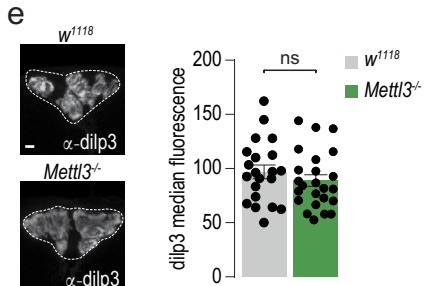


Extended Data Fig. 1| **The effects of Mettl3 KD on energy homeostasis are not developmental.** (a) Quantification of Mettl3 mRNA from heads of control $nSyb > w^{III8}CS$ (n = 3 sets of 20 flies) and $nSyb > Mettl3^{RNAi}$ flies (n = 6 sets of 20 flies). Unpaired two-tailed Student's t-test, p = 0.045. (b) Triglyceride levels normalized

to protein in male control ($Tubulin\text{-}GAL80^{ts}$, dilp2-GAL4/+) and $Tubulin\text{-}GAL80^{ts}$; $dilp2\text{-}Mettl3^{RNAi}$ flies. n=8, 6 pools of two flies. Unpaired two-tailed Student's t-test, p=0.0003. Error bars are SEM. * p<0.05, ** p<0.005.

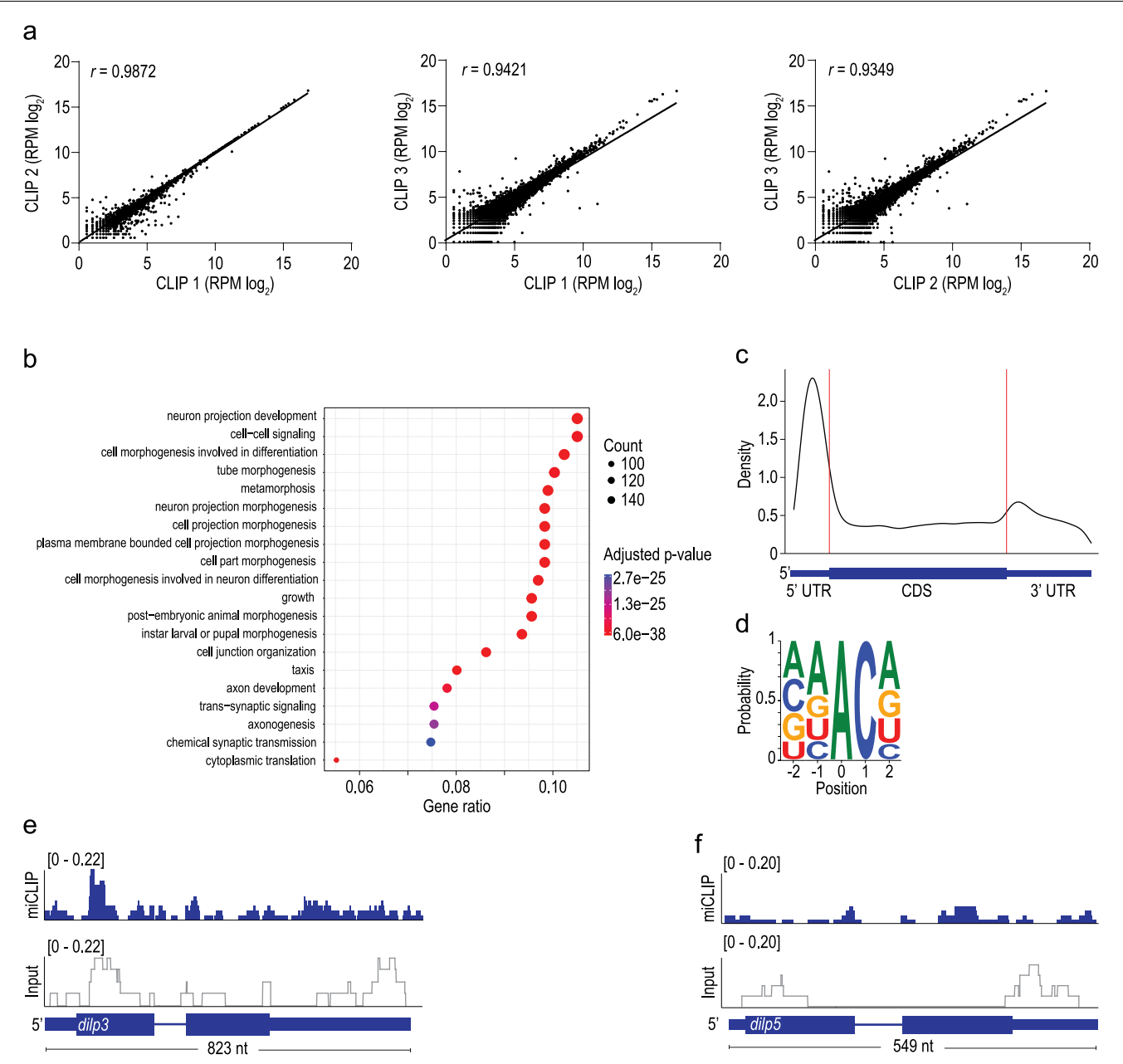






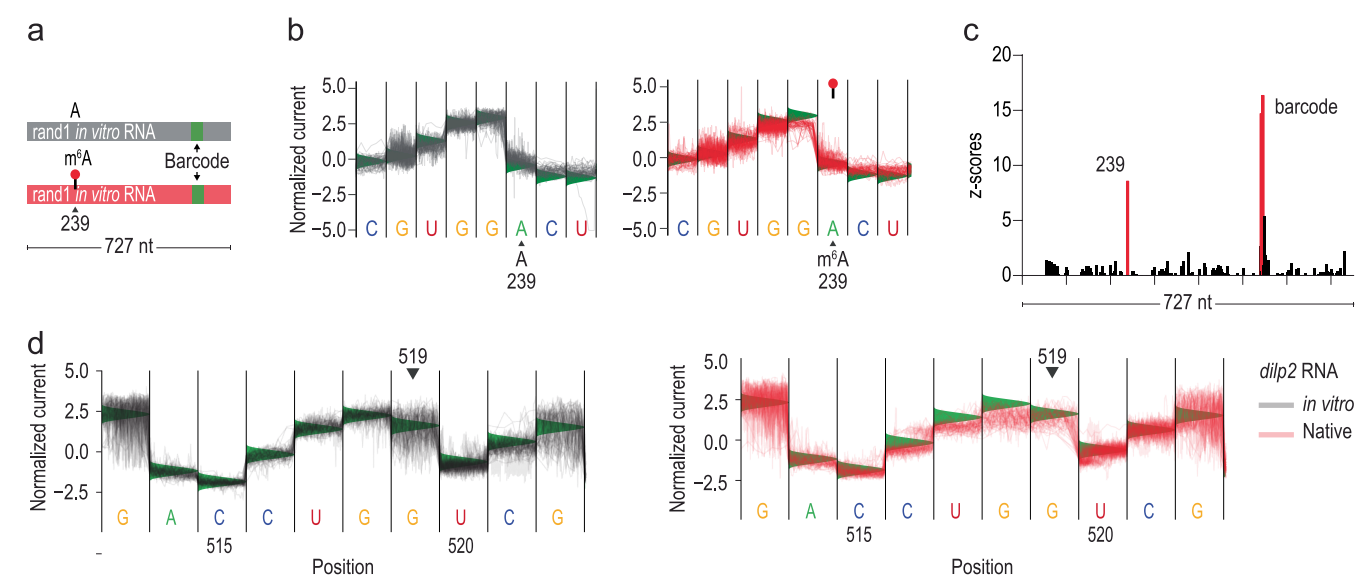
Extended Data Fig. 2 | **Additional phenotyping of Mettl3 mutants.** (**a**, **b**, **c**) Quantification of (a) dilp2, (b) dilp3, and (c) dilp5 mRNA from heads of control ($w^{III8}CS$) and $Mettl3^{-/-}$ mutant flies. n = 6 sets of 20 flies. Unpaired two-tailed Student's t-test; p = 0.594 (a), p = 0.778 (b), and p = 0.073 (c). (**d**) Quantification of insulin cells n = 3 brains. Unpaired two-tailed Student's t-test, p = 0.374. (**e**)

Representative confocal images of immunofluorescence of dilp3 protein in control ($w^{III8}CS$) and $Mettl3^{-/-}$ mutant flies. Scale bar, 20um. Quantification of median dilp3 fluorescence of individual insulin-producing cells from (d), n = 6 brains per genotype. Unpaired two-tailed Student's t-test, p = 0.333. Error bars are SEM. ns = not significant.



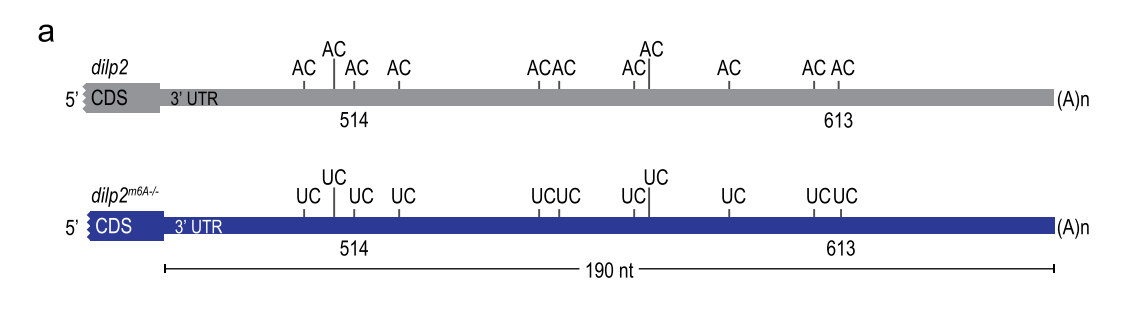
Extended Data Fig. 3 | Reproducibility of biological CLIP replicates. (a) Correlation plots of \log_2 normalized reads per CLIP peak. Each dot represents a CLIP peak found in all three biological replicates. Pearson's correlation coefficient (r). (b) Gene ontology (GO) enrichment analysis of genes that harbor a CLIP peak. Circle size represents the number of genes with CLIP peaks in the corresponding GO categories. The color represents the significance of the

enrichment (Benjamini–Hochberg corrected p-value from Gene Set Enrichment Analysis (GSEA)). (\mathbf{c}) Metagene plot of CLIP peaks from D. melanogaster head mRNA. Representing the position of 4,506 CLIP peaks. (\mathbf{d}) The sequence context of 5,485 cross-linked mutational sites (CIMS) contained within CLIP peaks. (\mathbf{e} , \mathbf{f}) miCLIP (blue) and input (gray) traces mapped to the dilp3 (\mathbf{e}) and dilp5 (\mathbf{f}) loci (\underline{R} eads \underline{P} er \underline{M} illion mapped reads, RPM).



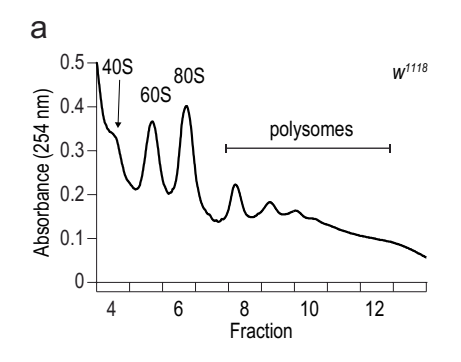
Extended Data Fig. 4 | **Direct RNA sequencing of in vitro transcribed control RNAs and dilp2 RNA.** (a) Schematic of the randomly generated random-1 (rand1) invitro transcribed RNAs. The RNAs were transcribed with A (gray) and m⁶A (red). The sequences were identical except for the 6 nt molecular barcode depicted by the green block to distinguish between the unmethylated and methylated RNA unambiguously. (b) Normalized direct RNA sequencing signal derived from invitro transcribed RNA with A (gray) and with m⁶A (red). n = 50 reads plotted. Green triangles represent the expected current level based on

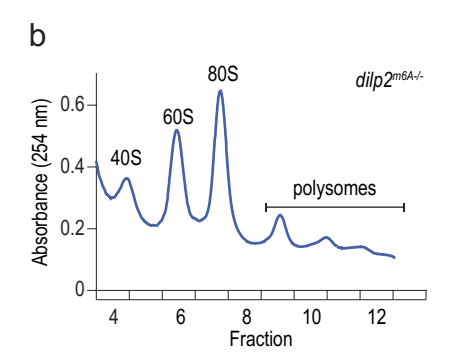
the base calling mode (see Methods). (c) EpiNano significance trace across the $\it in vitro$ transcribed RNA sequence. Significant position 239 (red) corresponds to the base following the methylated A (238). Other significant bases labeled 'barcode' correspond to the green barcode in (a). (d) Normalized direct-RNA sequencing signal derived from $\it in vitro$ transcribed $\it dilp2$ RNA (left, gray, n = 50 reads) and native $\it dilp2$ mRNA from fly heads (right, red n = 50 reads) of the region corresponding to the miCLIP peak in (Fig. 2a). Green triangles represent the expected current level based on the base calling model.

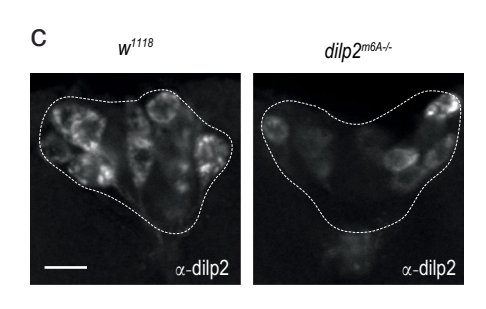


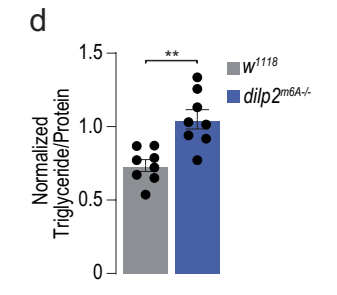


Extended Data Fig. 5 | **Creation of dilp2m6A mutant flies.** (a) Diagram of CRISPR strategy to replace 11 AC dinucleotides in 3' UTR of the dilp2 transcript ($dilp2^{m6A-/-}$ gray). (b) Sanger sequencing of genomic DNA from positive transgenic line 364-4 showing all 11 AC dinucleotides replaced with UC.



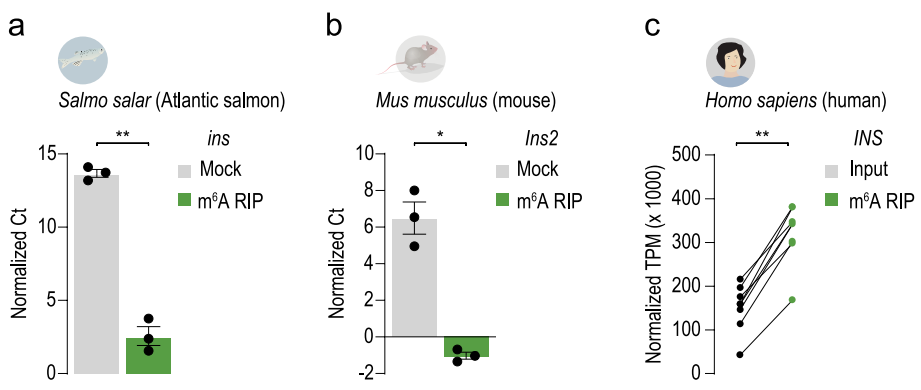






Extended Data Fig. 6 | **Polysome profiles of control and dilp2m6A-/- mutant flies. (a, b)** Representative polysome profile from sucrose gradient of (a) control (w^{III8}) and (b) $dilp2^{m6A-/-}$ mutant fly heads in Fig. 2c. (c) Representative confocal images of immunofluorescence of dilp2 protein in control $(w^{III8}CS)$ and $Mettl3^{-/-}$

mutant flies. Scale bar, 20um. (**d**) Triglyceride levels normalized to protein in control (w^{III8}) and mutant $dilp2^{m64-f-}$ flies. n=8. Error bars SEM. Unpaired two-sided Student's t-test, p=0.001. ** p<0.005.



Extended Data Fig. 7 | **Vertebrate insulin mRNA is enriched by m6A RIP. (a, b)** Quantification of salmon *ins* (a) and mouse *Ins2* (b) mRNA by qPCR from mock-treated or m^6A RIP samples of pancreatic tissue. n=3 salmon and n=3 of groups of two male mice. Error bars SEM. Unpaired two-tailed Student's t-test, p<0.0001

(a) and p = 0.001 (b). (c) Normalized Transcripts Per Kilobase Million (TPM) counts of RNA-sequencing reads from the human insulin (INS) gene 6 . Paired two-tailed Student's t-test p < 0.0001. *p < 0.05, ** p < 0.005.

nature portfolio

Corresponding author(s):	Monica Dus
Last updated by author(s):	May 8, 2023

Reporting Summary

Nature Portfolio wishes to improve the reproducibility of the work that we publish. This form provides structure for consistency and transparency in reporting. For further information on Nature Portfolio policies, see our <u>Editorial Policies</u> and the <u>Editorial Policy Checklist</u>.

<.	トつ	1	ıc:	ŀι	CS
J	ιa	ı.	I.O.	LΙ	LJ

For	statistical analyses, confirm that the following items are present in the figure legend, table legend, main text, or Methods section.
n/a	Confirmed
	The exact sample size (n) for each experimental group/condition, given as a discrete number and unit of measurement
	A statement on whether measurements were taken from distinct samples or whether the same sample was measured repeatedly
	The statistical test(s) used AND whether they are one- or two-sided Only common tests should be described solely by name; describe more complex techniques in the Methods section.
X	A description of all covariates tested
	A description of any assumptions or corrections, such as tests of normality and adjustment for multiple comparisons
	A full description of the statistical parameters including central tendency (e.g. means) or other basic estimates (e.g. regression coefficient AND variation (e.g. standard deviation) or associated estimates of uncertainty (e.g. confidence intervals)
	For null hypothesis testing, the test statistic (e.g. <i>F</i> , <i>t</i> , <i>r</i>) with confidence intervals, effect sizes, degrees of freedom and <i>P</i> value noted Give <i>P</i> values as exact values whenever suitable.
\boxtimes	For Bayesian analysis, information on the choice of priors and Markov chain Monte Carlo settings
\boxtimes	For hierarchical and complex designs, identification of the appropriate level for tests and full reporting of outcomes
	\leq Estimates of effect sizes (e.g. Cohen's d , Pearson's r), indicating how they were calculated
	Our web collection on <u>statistics for biologists</u> contains articles on many of the points above.

Software and code

Policy information about availability of computer code

Data collection

Direct RNA sequencing acquisition: Oxford Nanopore MinKNOW (21.06.0) Immunofluorescence acquisition: Olympus Fluoview (04.02.01.20) qPCR acquisition: Applied Biosystems StepOne Software (v2.3) Sucrose gradient absorbance acquisition: Brandel Peak Chart (2.08) Colormetric assay acquisition: Tecan Spark Control (3.0)

Data analysis

Direct RNA sequencing base calling: Oxford Nanopore Guppy (v 3.1.5)
Direct RNA sequencing transcriptome mapping: MiniMap2 (v 2.17)
Direct RNA sequencing modification identification: EpiNano-Error (v 1.2)
Direct RNA sequencing visualization: Tombo (1.5)
Samtools (1.9)
bedtools2 (2.30.0)

Microscopy visualization and quantification: Fiji (ImageJ 1.53f51)

De-multiplexing Solexa sequencing reads: Bcl2fastq2 Conversion Software (Illumina)

Adapter trimming Solexa sequencing reads: fastx_clipper (0.0.14)

Mapping Solexa sequencing reads: Star (v 2.7.5a)

Removing duplicated reads from Solexa sequencing reads: remove_duplicated_reads_from_fastq_testing.pl (v 0.1.0) (https://github.com/dwilinski/m6A-fly-insulin.git)

 $Removing\ direct-RNA\ sequencing\ reads:\ filter_sam_on_deletions.pl\ (V\ 0.1.0)\ (https://github.com/dwilinski/m6A-fly-insulin.git)$

Defining CLIP peaks: Piranha (v 1.2.1)

Metagene visualization of CLIP data: MetaPlotR (v 1.0)

Visualization of CLIP data: weblogo (v 2.8.2)

Gene Set Enrichment Analysis: ClusterProfiler R package version (4.2.2) Bioconductor package "Genome Wide Annotations for Fly" (v 3.8.2) for GESA

Visualization of Sanger sequencing: Benchling software (2021)

For manuscripts utilizing custom algorithms or software that are central to the research but not yet described in published literature, software must be made available to editors and reviewers. We strongly encourage code deposition in a community repository (e.g. GitHub). See the Nature Portfolio guidelines for submitting code & software for further information.

Data

Policy information about availability of data

All manuscripts must include a data availability statement. This statement should provide the following information, where applicable:

- Accession codes, unique identifiers, or web links for publicly available datasets
- A description of any restrictions on data availability
- For clinical datasets or third party data, please ensure that the statement adheres to our policy

All data are available in the main text or supplementary materials. RNA-sequencing reads were deposited in Gene Expression Omnibus accession number GSE207547. dilp2 3'UTR mutant flies are available upon request. Ensembl D. melanogaster genome (BDGP6.32) genome. D. melanogaster genome sequence accession number (BDGP6.32), Mus musculus Ins2 sequence (NM_001185083.2), and Salmo salar ins sequence (XM_014198195.2).

Human research participants

Policy information about studies involving human research participants and Sex and Gender in Research.

Reporting on sex and gender	NA
Population characteristics	NA
Recruitment	NA
Ethics oversight	NA

Note that full information on the approval of the study protocol must also be provided in the manuscript.

Field-specific reporting

Please select the one below that is the best fit for your	research. If you are not sure, read the	e appropriate sections before making your selection	on.

Life sciences Behavioural & social sciences Ecological, evolutionary & environmental sciences

For a reference copy of the document with all sections, see nature.com/documents/nr-reporting-summary-flat.pdf

Life sciences study design

All studies must disclose on these points even when the disclosure is negative.

Sample size

Sample sizes were determined based on norms of the field. Tennessen, J. M., Barry, W. E., Cox, J. & Thummel, C. S. Methods for studying metabolism in Drosophila. Methods 68, 105–115 (2014). May, C. E. et al. High Dietary Sugar Reshapes Sweet Taste to Promote Feeding Behavior in Drosophila melanogaster. Cell Rep. 27, 1675–1685.e7 (2019). Kan, L. et al. A neural m6A/Ythdf pathway is required for learning and memory in Drosophila. Nat. Commun. 12, 1458 (2021). In one case, Mettl3-/-;dilp2>Mettl3 flies only had 3 biological replicates because we did not obtain enough flies. One direct-RNA sequencing experiment was conduced for each condition/genotype because of cost. Biological replicates for meRIP-qPCR were limited for Atlantic salmon (n=3) and mouse experiments (n=3) because of limited material.

Data exclusions No data were excluded from analysis

Replication

All attempts at replication were successful. TAGs data were replicated interdependently at least twice. All IF data were replicated interdependently across days. All polysome fractions were replicated across days. Polysome-qPCR biological replicates were run on a separate plates with technical replicates. CLIP data were conducted as one set and not replicated. Direct-RNA sequencing data were not replicated.

Randomization

All samples/organisms were allocated into experimental groups randomly

Blinding

All IF experiments that required manual ROI determinations were blinded by the investigators. Investigators were not blinded to group allocation and analysis since assignment of samples to different experimental groups was random or based on genotype.

Reporting for specific materials, systems and methods

We require information from authors about some types of materials, experimental systems and methods used in many studies. Here, indicate whether each material, system or method listed is relevant to your study. If you are not sure if a list item applies to your research, read the appropriate section before selecting a response.

Materials & exper	imental systems – Met	hods	
n/a Involved in the study		Involved in the study	
Antibodies		ChIP-seq	
Eukaryotic cell	lines 🔀 🛚	Flow cytometry	
Palaeontology	and archaeology	MRI-based neuroimaging	
Animals and ot	her organisms		
Clinical data			
Dual use resear	rch of concern		
1			
Antibodies			
Antibodies used	rat anti-dilp2 (Pierre Léopold) refer rabbit anti-dilp3 (Patrick Callaerts) goat anti-rat Alexa Fluor 647 (Invitr goat anti-rabbit Alexa Fluor 488 (In mouse anti-Flag monoclonal antibo	PA2172 reference in text ogen, A-21247) vitrogen, A-11008)	
Validation	Dilp2 and dilp3 antibodies were previously validated in the literature and by subsequent investigators. The antibodies stained the expected regions of the fly brain. Dilp2 antibody was validated by expressing dilp2 in Kurs6 neurons which do not endogenously express dilp2 and probed by immunofluorescence. Only when dilp2 was over-expressed not when dilp5 was over-expressed did they find immunofluorescence in the Kurs6 neurons (Figure S1). (Géminard, Charles et al. Remote Control of Insulin Secretion by Fat Cells in Drosophila. Cell Metabolism, Volume 10, Issue 3, 199 - 207) To validate the Dilp3 antibody, the authors used dilp3 knockout flies and observed a loss of immunofluorescence compared to control flies in insulin producing cells (Figure S9). (Buhler, Kurt et al. Growth control through regulation of insulin signalling by nutrition-activated steroid hormone in Drosophila. Development 1 November 2018; 145 (21): dev165654.)		
and the second s			

Animals and other research organisms

Policy information about <u>studies involving animals</u>; <u>ARRIVE guidelines</u> recommended for reporting animal research, and <u>Sex and Gender in Research</u>

Laboratory animals	Drosophila, w[1118]CS
	Drosophila, w[1118]
	Drosophila, Ime4null (Mettl3)
	Drosophila, UAS-Ime4-HA/Cyo
	Drosophila, UAS-Mettl3RNAi: y[1] v[1]; P{y[+t7.7] v[+t1.8]=TRiP.GL01126}attP2/TM3, Sb[1]
	Drosophila, Dilp2-GAL4: w[*]; P{w[+mC]=llp2-GAL4:R}2/CyO
	Drosophila, nSyb-GAL4-2.1
	Drosophila, Tubulin-GAL80, dilp2-GAL4: w[*];Dilp2R-Gal4,TubP-Gal80[ts]/Cyo; +
	Drosophila dilp2m6A: w[1118];;Dilp2[m6A]/TM6C
	(All flies were 3-10 days old)
	Atlantic salmon (Salmo salar) (male post smolt and are about 2 years old)
	Male mice Vil-Cre backcrossed to C57 9x (male, 1.5 months old)
Wild animals	Study did not involve wild animals
Reporting on sex	For practical reasons some experiments were done on both sexes together. For example, for some experiments (CLIP, polysome profiling) it was impractical to segregate by sex when a large number of animals were required to obtain sufficient tissue. Otherwise experiments were conducted on males.
Field-collected samples	Study did not involve field-collected samples
Ethics oversight	The mouse tissue was obtained from University of Michigan Islet Isolation core and the salmon pancreatic tissue was obtained from a collaborator so no animal care and use oversight was required.

Note that full information on the approval of the study protocol must also be provided in the manuscript.